# Molecular Dynamics Simulations of MRI-Relevant $Gd^{III}$ Chelates: Direct Access to Outer-Sphere Relaxivity

**Alain Borel, Lothar Helm, and André E. Merbach*[a]**

**Abstract:** The structure and dynamics of the surrounding water were studied through molecular dynamics (MD) simulations for several $Gd^{III}$ polyaminocarboxylate and polyaminophosphonate complexes in aqueous solution. The radial distribution functions (rdf) show that a few water molecules are bonded to the ligand through hydrogen bonds to hydrophilic groups such as carboxylates and phosphonates. Residence times are of the order of 20–25 ps for the polyaminocarboxylate and 56 ps for the polyaminophosphonate chelates. No preferred orientation or bonding of water molecules is observed in the hydrophobic region of the anisotropic macrocyclic complexes. Our rdf allow calculation of the outer-sphere contribution to the nuclear magnetic resonance dispersion (NMRD) profiles using Freed's finite differences method, including electronic relaxation. The results show that the commonly used analytical force-free model is only an empirical relationship. When experimental outer-sphere NMRD profiles are available ($[Gd(teta)]^-$ and $[Gd(dotp)]^{5-}$ (teta = *N*,*N*′,*N*″,*N*‴-tetracarboxymethyl-1,4,8,11-tetraazacyclotetradecane; dotp = *N*,*N*′,*N*″,*N*‴-tetraphosphonatomethyl-1,4,7,10-tetraazacyclododecane) the calculated curves are in good agreement. In the case of $[Gd(teta)]^-$, the comparison with the experimental NMRD profile has led us to predict a very fast electronic relaxation, which has been confirmed by the EPR spectrum.

**Keywords:** chelates · gadolinium · magnetic resonance imaging · molecular dynamics · relaxivity

## Introduction

Gadolinium(III) complexes are used routinely as contrast agents in magnetic resonance imaging (MRI). Contrast improvement is a consequence of the enhancement of the water proton magnetic relaxation rate in tissues through interactions with the seven unpaired f electrons of the $Gd^{III}$ center. The relaxation rate enhancement at a fixed $[Gd^{3+}]$ (1 mM) concentration (relaxivity) is commonly divided into two contributions: inner-sphere (due to protons of water molecules directly coordinated to the metal and transmitted to the bulk by chemical exchange) and outer-sphere (dipolar interactions through space with surrounding water molecules).[1, 2] The former is well understood on the microscopic scale, but the latter is usually described using Freed's approximate force-free model,[3, 4] in which the only parameters are the relative diffusion coefficient between the paramagnetic center and the water molecules, and the distance of closest approach for the protons. This simple relation has been questioned recently,[5, 6] with the introduction of a "second coordination sphere". To obtain a more detailed view, we have used molecular dynamics (MD) simulations to study the structure and dynamics of water around several $Gd^{III}$ complexes: three with macrocyclic ligands, $[Gd(teta)]^-$ (teta = *N*,*N*′,*N*″,*N*‴-tetracarboxymethyl-1,4,8,11-tetraazacyclotetradecane), $[Gd(dota)(H_2O)]^-$ (dota = *N*,*N*′,*N*″,*N*‴-tetracarboxymethyl-1,4,7,10-tetraazacyclododecane), and $[Gd(dotp)]^{5-}$ (dotp = *N*,*N*′,*N*″,*N*‴-tetraphosphonatomethyl-1,4,7,10-tetraazacyclododecane), and two with acyclic ligands, $[Gd(dtpa)(H_2O)]^{2-}$ (dtpa = *N*,*N*,*N*′,*N*″,*N*″-pentacarboxymethyl-1,4,7-triazapentane), and [Gd(dtpa-bma)($H_2O$)] (dtpa-bma = *N*,*N*″-bis[(*N*-methylcarbamoyl)methyl]-*N*,*N*′,*N*″-tris-carboxymethyl-1,4,7-triazapentane) . Two of these complexes ($[Gd(teta)]^-$ and $[Gd(dotp)]^{5-}$) have no inner-sphere water, allowing direct experimental study of the outer-sphere relaxivity. Comparison of the theoretical and experimental results for these two compounds is therefore an important step in understanding the relaxivity of MRI contrast agents beyond the inner sphere.

This work is part of an ongoing effort to study the properties of transition metal and lanthanide ions and their complexes in aqueous solution using computational methods. Earlier studies by our group included MD simulations of trivalent lanthanide ions[7–9] and the chromium(III) heaxaaqua

[a] Prof. A. E. Merbach
Institut de Chimie Minérale et Analytique
Université de Lausanne
BCH, 1015 Lausanne (Switzerland)
Fax: (+41) 21-692-38-75
E-mail: andre.merbach@icma.unil.ch

Supporting information for this article is available on the WWW under http://www.wiley-vch.de/home/chemistry/ or from the author.



0947-6539/01/0703-0600 $ 17.50+.50/0

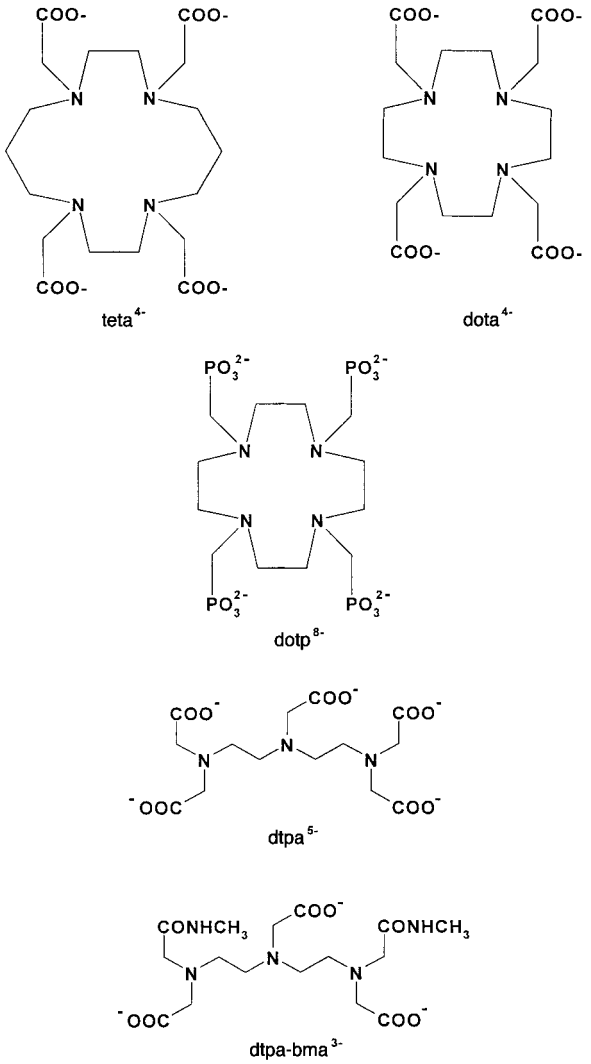


complex.[10] In all these systems, the existence of a labile coordination sphere (first sphere for the lanthanides, second sphere for chromium) was well established by experimental methods such as $^{17}O$ NMR and the agreement between experimental and computational results was found to be fairly good. No direct structural and dynamic data were available for the outer-sphere MRI contrast agents and related complexes. Our goal was to obtain such information through classical MD simulations.

The magnetic property of interest for potential MRI contrast agents is the total relaxivity $r_1$ itself. As it stands, Freed's force-free model has been an important tool for estimating the outer-sphere contribution to relaxivity. Our aim was not only to confirm, or otherwise, the validity of this model, but also to calculate the outer-sphere relaxivity contribution directly from our simulations.

Computer modeling has been used in the past to investigate the properties of gadolinium MRI contrast agents. Molecular mechanics,[11–13] Hartree–Fock,[14, 15] and density functional theory[16] have been applied, generally with an emphasis on the structure and energy of these compounds. In this study we were interested in the interaction of these complexes with the surrounding water molecules so the main purpose of our force field was to describe intermolecular forces using ad hoc parameters derived from ab initio calculations.

## Computational Methods

**Outline of the simulation**

**Force field parameters**: To achieve a proper description of the electrostatic potential, which is essential to simulations involving ions and polar molecules, we calculated partial atomic charges for the various complexes by the Merz–Kollman method[17] as implemented in the Gaussian 94 package.[18] This method outputs atomic charges by fitting them to the electrostatic potential at a fixed distance through a dielectric medium. Ab initio calculations were performed on the four available crystal structures[19–22] at the 6–31G** level (H, C, N, O, P) with pseudopotentials according to Dolg and Stoll[23] accounting for relativistic corrections in the treatment of the core electrons of Gd. The calculated charges (Table 1) were then averaged over all atoms of the same type. For the $[Gd(dotp)]^{5-}$ complex no experimental crystal structure was available, so we calculated an optimized structure (Table 2) using the density functional theory (DFT) program ADF.[24] This calculation was performed at the nonlocal density approximation (NLDA) with Becke[25] and Perdew[26] gradients for the exchange and correlation functionals. The basis set was Slater type atomic

Table 1. Atomic charges derived from ab initio calculations for $[Gd(L^{-n})(H_2O)_x]^{3-n}$.

| | $[Gd(teta)]^-$ | $[Gd(dota)(H_2O)]^-$ | $[Gd(dotp)]^{5-}$ | $[Gd(dtpa)(H_2O)]^{2-}$ | $[Gd(dtpa-bma)(H_2O)]$ |
|---|---|---|---|---|---|
| Gd | 2.17 | 2.12 | 2.35 | 2.30 | 1.96 |
| N amine | −0.10 | −0.81 | −0.25 | 0.20 | 0.00[a]/0.60 |
| C ethylene bridge | −0.15 | −0.042 | −0.18 | 0.00 | 0.00[a]/−0.20[b] |
| H ethylene bridge | 0.09 | 0.13 | 0.14 | 0.03 | 0.10 |
| C methyl/methylene | −0.55 | 0.02 | −0.50 | −0.50 | −0.20 |
| H methylene | 0.20 | 0.14 | 0.14 | 0.03 | 0.13 |
| C carboxylate/P | 1.00 | 0.81 | 1.40 | 0.90 | 0.90 |
| $O_c$ carboxylate/phosphonate (coordinating) | −0.85 | −0.81 | −1.00 | −0.90 | −0.65[c] / −0.80[d] |
| $O_f$ carboxylate/phosphonate (free) | −0.75 | −0.71 | −0.98 | −0.80 | −0.70 |
| O inner-sphere water | – | −0.60 | – | −1.00 | −0.80 |
| H inner-sphere water | – | 0.30 | – | 0.50 | 0.40 |
| N amide | – | – | – | – | −0.45 |
| O amide | – | – | – | – | −0.65 |
| H amide | – | – | – | – | 0.35 |
| C N-methyl | – | – | – | – | −0.25 |
| X-ray structure | ref. [19] | ref. [20] | N/A[e] | ref. [21] | ref. [22][e] |

[a] Central. [b] Terminal. [c] Amide group. [d] Carboxylate group. [e] Full structure available as Supporting Information.

Table 2. Selected distances from the DFT-optimized structure of $[Gd(dotp)]^{5-}$.

| Distance | Å |
|---|---|
| Gd–O | 2.390 ± 0.018 |
| Gd–N | 3.041 ± 0.055 |
| C–P | 1.908 ± 0.007 |
| P–O | 1.577 ± 0.018 |

orbitals (STO) with triple zeta and polarization, using the smallest possible relativistic core for each element (He core for O, C, N; Ne core for P; Xe core for Gd).

The Merz–Kollman approach leads to a good representation of the electrostatic potential at the molecular surface but only to a rather poor description of intramolecular electrostatic interactions. In our systems, the bonding of negatively charged donor groups such as carboxylates, and of inner-sphere water, to the metal center was found to be especially problematic. To avoid undesired behavior during the simulation (such as the substitution of a carboxylate group by solvent molecules or departure of the inner-sphere water molecule) we introduced bonds of crystallographic length for the $Gd^{III}$ coordination. We can justify this treatment because the complexes can be considered rigid on the molecular dynamics time scale. Using $^{17}O$ NMR, Powell et al.[27] found that the inner-sphere residence time of water molecules was of the order of microseconds for the fastest exchanging complexes in our study, $[Gd(dota)(H_2O)]^-$ and $[Gd(dtpa)(H_2O)]^{2-}$. The $[Gd(dota)(H_2O)]^-$ complex is present in solution as a mixture of a major *M* (80%) and a minor *m* (20%) isomer with different structures.[28] Whereas the two isomers display significant differences in their first coordination sphere, we expected their influence on the second shell to be a minor one. Therefore we used the *M* isomer structure, which we may also consider to be a rigid molecule as the exchange rate between the isomers is slow throughout the lanthanide series even on the $^1H$ NMR time scale.

We used the TIP3P model of Jorgensen et al.[29] for water molecules, and the van der Waals parameters for $Gd^{3+}$ published by Kowall et al.[7–9] Other parameters for the force field were taken from the GROMOS86[30] package.

**Computation details**: Molecular dynamics runs were performed in the NTP ensemble using the GROMOS86 program running on a Silicon Graphics workstation. Bond lengths for all molecules in the system were fixed by the SHAKE procedure;[31] temperature and pressure were conserved using Berendsen's algorithm.[32] For each system the solute molecule was immersed in an initial 25 Å × 25 Å × 25 Å cubic periodic box (35 Å × 35 Å × 35 Å for the highly charged $[Gd(dotp)]^{5-}$ complex). No counterions were included in the simulation. Although this might be inappropriate for the complexes with a high negative charge, it makes the analysis easier and more systematic when complexes with different ligands are being compared. Other important parameters are summarized in Table 3.

## Results and Discussion

### Complexes with macrocyclic ligands

**Structural results**: The radial distribtion function $g(r)$ (rdf) for complexes with macrocyclic ligands ($teta^{4-}$, $dota^{4-}$, and $dotp^{8-}$) was calculated as an average over the simulation configurations of the ratio of the local density of a given particle (in our case water molecules, given by their O or H atoms) at a distance $r$ from a given center (for example the $Gd^{III}$ ion) to the overall density [Eq. (1)].

$$g(r) = \frac{n(\mathrm{r})}{4\pi r^2 \Delta r \rho} \quad (1)$$

In the case of $[Gd(dota)(H_2O)]^-$, the inner-sphere water molecule was excluded from the gadolinium–solvent water radial distribution function $g(r)$ as given by water O and H atoms, respectively (Figure 1), since its distance from the metal was constrained in the simulations. For all complexes, the rdf values for both Gd–H and Gd–O display a rather well-defined peak in the 3.0–5.0 Å region (Table 4), which shows that the behavior of the water between these distances is

Table 3. Overview of simulation parameters for $[Gd(L^{-n})(H_2O)_x]^{3-n}$.

| | $[Gd(teta)]^-$ | $[Gd(dota)(H_2O)]^-$ | $[Gd(dotp)]^{5-}$ | $[Gd(dtpa)(H_2O)]^{2-}$ | $[Gd(dtpa\text{-}bma)(H_2O)]$ |
|---|---|---|---|---|---|
| number of water molecules | 500 | 490 | 1426 | 498 | 498 |
| equilibration time [ps] | 32 | 32 | 32 | 32 | 32 |
| simulation time [ps] | 262 | 262 | 524 | 262 | 262 |
| stored configurations | 4096 | 4096 | 8192 | 4096 | 4096 |
| cutoff radius [Å] | 11.0 | 11.0 | 16.0 | 10.5 | 11.0 |
| $\tau_T$ [ps][a] | 0.01 | 0.01 | 0.01 | 0.01 | 0.01 |
| $\tau_P$ [ps][a] | 0.05 | 0.05 | 0.05 | 0.05 | 0.05 |
| average density [g cm$^{-3}$] | 1.0315 | 1.0227 | 1.0315 | 1.0200 | 1.0486 |
| temperature [K] | 285 | 285 | 285 | 285 | 285 |
| pressure [atm] | 1 | 1 | 1 | 1 | 1 |

[a] Relaxation times for temperature and pressure in the algorithm of Berendsen.

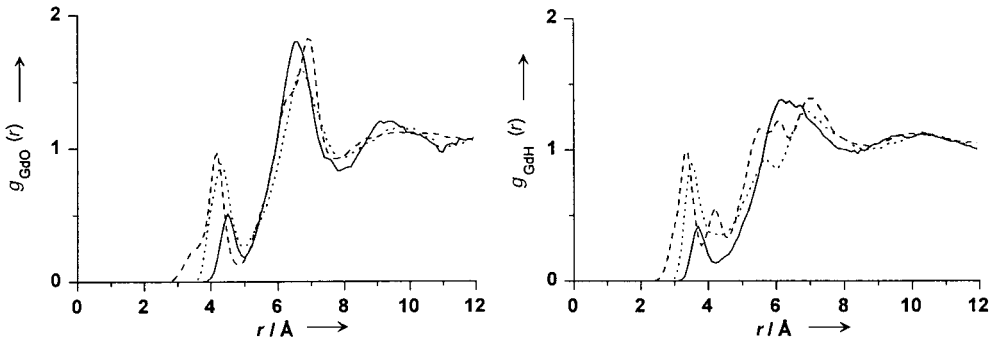


Figure 1. Radial distribution functions for water a) O atoms and b) H atoms around Gd of $[Gd(teta)]^-$ (——), $[Gd(dota)(H_2O)]^-$ (····) and $[Gd(dotp)]^{5-}$ (- - - -).



0947-6539/01/0703-0602 $ 17.50+.50/0 *Chem. Eur. J.* **2001**, *7*, No. 3

Table 4. The rdf peak parameters and corresponding coordination number $q$ for water oxygen and hydrogens.

| Complex | O peak position [Å] | Half height width [Å] | $q_O$ | H peak position [Å] | Half height width [Å] | $q_H$ |
|---|---|---|---|---|---|---|
| $[Gd(teta)]^-$ | 4.5 | 0.5 | 2.5 | 3.7 | 0.5 | 2.6 |
| $[Gd(dota)(H_2O)]^-$ | 4.3 | 1.0 | 5.1 | 3.5 | 0.65 | 6.4 |
| $[Gd(dotp)]^{5-}$ | 4.2 | 0.3 | 4.6 | 3.4 | 0.3 | 5.3 |
| $[Gd(dtpa)(H_2O)]^{2-}$ | 4.1 | 1.0 | 8.6 | 3.4 | 1.0 | 12.8 |
| $[Gd(dtpa\text{-}bma)(H_2O)]$ | 4.1 | (0.8) | 5.0 | 3.3 | (0.5) | 7.0 |

distinct from that of the bulk water. The relative positions of the H and O peaks indicate that water H atoms are involved in bonding to the solute molecule. By integrating $g(r)$ from 0 to the first minimum of the curve, we can define coordination numbers $q_O$ and $q_H$ for the O and H atoms respectively in the second coordination shell. This number is too small ($q_O = 2$–5) for the whole complex to be encompassed by a complete hydration sphere. Therefore a more detailed analysis was required.

The axial symmetry of the $[Gd(teta)]^-$, $[Gd(dota)(H_2O)]^-$, and $[Gd(dotp)]^{5-}$ complexes allows us to divide space around the complex into two regions, one hydrophilic (containing the carboxylates/phosphonates) and one hydrophobic (containing the macrocycle), as in Figure 2. The dividing plane is perpendicular to the main rotation axis, which can be described adequately by the vector joining the $Gd^{III}$ ion and the center of mass of the eight carboxylate O atoms. Thus we can distinguish water molecules in both regions and observe possible differences between them. We calculated the partial rdf in both the hydrophilic (carboxylate/phosphonate) and the hydrophobic (azacycle) regions. The water molecules responsible for the hydration peak are located in only the carboxylate/phosphonate hemisphere of the complexes (Figure 3). Bonding to the carboxylate/phosphonate O atoms was confirmed by the rdf around these atoms (Figure 4). A sharp peak in the rdf for both the hydrogen and oxygen was observed (with a maximum at $r = 1.6$ Å for H and $r = 2.6$ Å for O). The closer H peak indicates hydrogen bonds between water and the carboxylate O atoms. The free carboxylate O atoms ($O_f$)

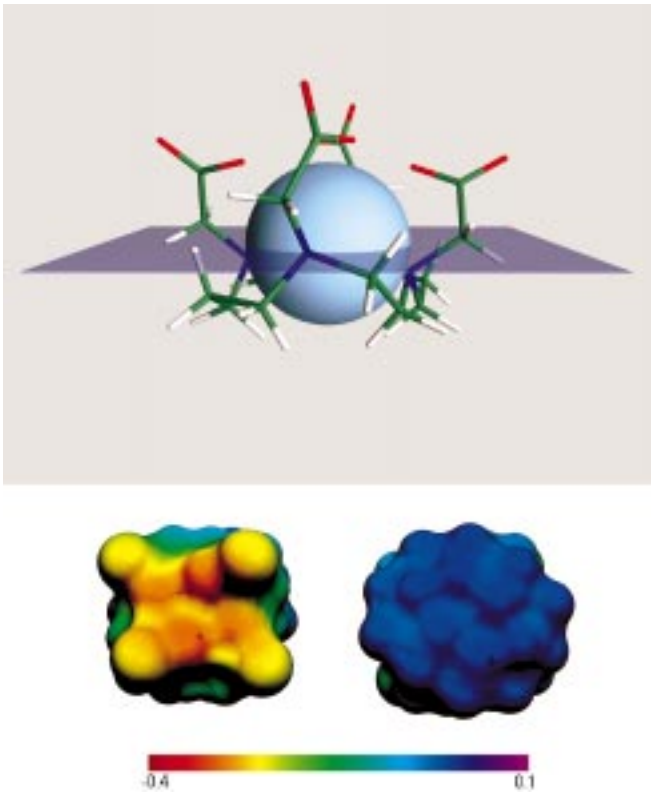


Figure 2. Top) Model of $[Gd(teta)]^-$, and division of the surrounding space into hydrophilic (above) and hydrophobic (below) hemispheres. Bottom) Electrostatic potential [au] at the molecular surface of $[Gd(teta)]^-$ in the hydrophilic (carboxylate, left) and hydrophobic (macrocycle, right) regions.

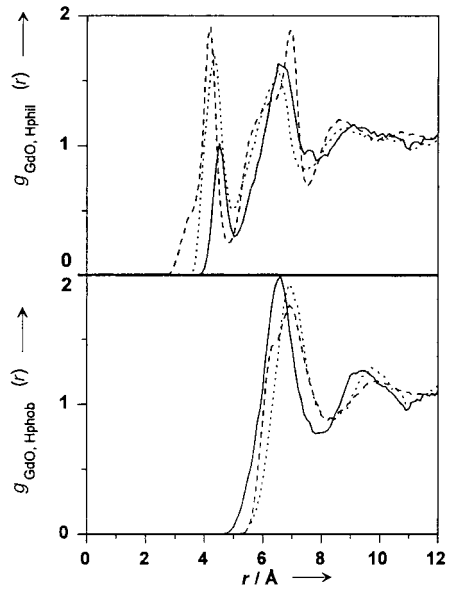


Figure 3. Partial rdf for water O atoms in the hydrophilic (top) and hydrophobic hemispheres (bottom) of $[Gd(teta)]^-$ (——), $[Gd(dota)(H_2O)]^-$ (····), and $[Gd(dotp)]^{5-}$ (----).

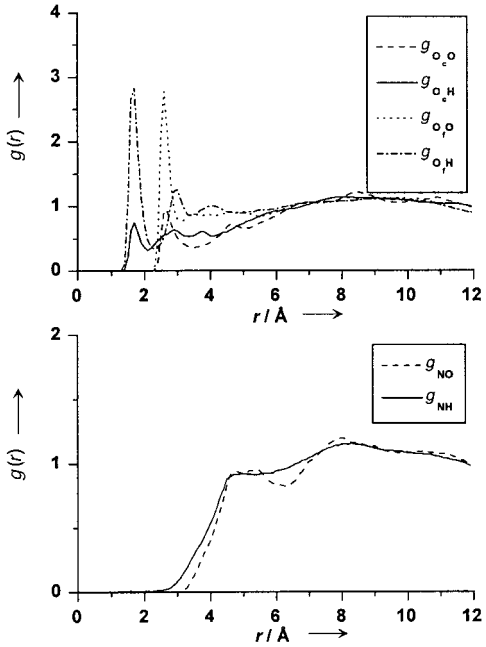


Figure 4. The rdf around carboxylate O atoms (top) and N atoms (bottom) of $[Gd(teta)]^-$. A distinction is made between O atoms bonded to the metal ion ($O_c$) and free O atoms ($O_f$).

are more accessible to the water H atoms than their coordinated counterparts ($O_c$), so they give rise to a greater number of hydrogen bonds and to a consequently higher rdf peak. However, no preferred orientation was apparent around the less accessible N atoms of the ring. The smooth rise of $g(r)$ from 0 to 1 at a distance of about 4 Å indicates a shielding of the N atoms by the shear volume of the neighboring macrocyclic C and H atoms, and there is essentially no difference between the H and O distributions. The $[Gd(dota)(H_2O)]^-$ and $[Gd(dotp)]^{5-}$ complexes display the same features.

Bonding of water molecules through their H atoms can also be shown by their dipole orientation, characterized by $\cos\Theta$ ($\Theta$ is the angle between the Gd–O vector and the water dipole; Figure 5). Figures 6 and 7 demonstrate that water molecules close to the metal center ($r_{GdO} < 5$ Å) are preferentially oriented with one or both of their H atoms toward the complex core ($\cos\Theta$ is close to $-1$, and the angle distribution remains narrow). At a greater distance water molecules are randomly oriented (the average $\cos\Theta$ is nearly zero and the distribution broadens, as shown by its standard deviation). This is consistent with the bonding of water protons to carboxylate/phosphonate oxygen. For $[Gd(dotp)]^{5-}$, $\cos\Theta$ rises again to less negative values when the metal–oxygen distance diminishes, the closest approach distance during the simulation being $r_{GdO} = 2.76$ Å, only 0.3 Å longer than the inner-sphere $r_{GdO}$ in $[Gd(dota)(H_2O)]^-$. The shoulder of the oxygen $g(r)$ curve in the 2.5–3.5 Å region in Figure 1a also supports the picture of one water molecule in the close vicinity of the metal. This event occurred very rarely, however, as only 0.2% of the stored configurations showed a water molecule closer than 2.9 Å from the metal. The integration of $g(r)$ from 0 to 3.5 Å only corresponds to 0.4 water O atoms. To say there is coordination of one inner-sphere water molecule would not be fully justified in this case, considering the rarity of the event.

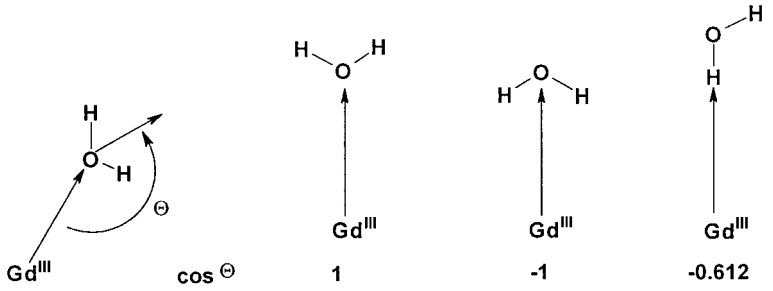


Figure 5. Orientation angle $\Theta$ and limiting values of $\cos\Theta$.

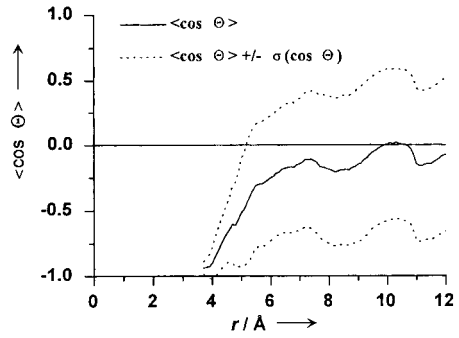


Figure 6. Average $\cos\Theta$ as a function of the metal–oxygen distance $r_{GdO}$ for $[Gd(teta)]^-$.

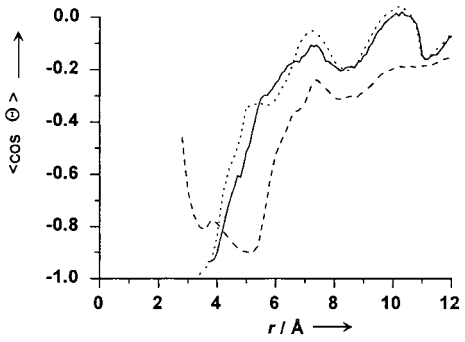


Figure 7. Average $\cos\Theta$ as a function of the metal–oxygen distance for $[Gd(teta)]^-$ (——), $[Gd(dota)(H_2O)]^-$ (····) and $[Gd(dotp)]^{5-}$ (----).

**Dynamic properties**: Water molecules located in the second coordination shell typically exchange with molecules from the bulk after an average residence time $\tau_M$, which can be calculated from the persisting coordination correlation function $n(t)$[33] [Eq. (2)], where $P_j$ is unity if water molecule $j$ is in

$$n(t) = \frac{1}{N}\sum_{i=1}^{N}\sum_{j} P_j(t_n, t, t^*) \qquad (2)$$

the coordination shell (defined in our case by the first minimum of the Gd–O rdf at 5.0 Å as an outer limit) at times $t_n$ and $t_n + t$ and is only allowed to leave this shell for small delays shorter than $t^*$. One can assume a decaying exponential form for this correlation function [Eq. (3)].

$$n(t) \cong q\exp\left(\frac{-t}{\tau_M}\right) \qquad (3)$$

By fitting Equation (3) to the calculated $n(t)$, one obtains the coordination number $q$ and the residence time $\tau_M$. However, the result depends on $t^*$ and should increase monotonically with this parameter. We used a canonical value of 2 ps for $t^*$.[33] The calculated parameters and the errors from the fit are given in Table 5.

Residence times obtained for $H_2O$ molecules in our second coordination shell are in the 20–25 ps range for the polyaminocarboxylate complexes (56 ps for the polyaminophosphonate-based $[Gd(dotp)]^{5-}$), indicating a fast exchange

Table 5. Second-shell hydration parameters from coordination correlation function $n(t)$.

| Complex | Hydration number $q$ | Residence time $\tau_M$ [ps] |
|---|---|---|
| $[Gd(teta)]^-$ | 1.9 | 24.3 |
| $[Gd(dota)(H_2O)]^-$ | 4.3 | 27.4 |
| $[Gd(dotp)]^{5-}$ | 4.3 | 56.1 |
| $[Gd(dtpa)(H_2O)]^{2-}$ | 6.9 | 20.3 |
| $[Gd(dtpa\text{-}bma)(H_2O)]$ | 4.4 | 22.5 |



0947-6539/01/0703-0604 $ 17.50+.50/0 *Chem. Eur. J.* **2001**, *7*, No. 3

with bulk water: in comparison, the second-sphere residence time of water molecules around the inert $[Cr(H_2O)_6]^{3+}$ complex has been determined both experimentally through $^{17}O$ NMR and theoretically through MD simulations to be over 120 ps,[10] whereas in their simulations Kowall et al.[9] showed a residence time of 12, 13, and 18 ps in the second shell of $Sm^{3+}$, $Nd^{3+}$, and $Yb^{3+}$, respectively. However, our values should be compared with these results only with extreme caution, as the hydrogen bonding of solvent water molecules to the complex proceeds through water O atoms in these aqua complexes. Our residence times are more properly compared with other results obtained for organic and biological molecules (4.8 ps for DMSO in a 1:2 DMSO–water mixture;[34] 3.9–7.7 ps for the alanine dipeptide;[35] 10–15 ps for ribose and phosphate O atoms on the *trp* operator double-stranded DNA fragment[36, 37]).

Our metal-centric second shell definition is open to criticism; indeed, another definition is quite possible for the presence function $P_j$ [Eq. (2)]. By studying the presence of water H atoms around carboxylate or phosphonate O atoms, the mean lifetime of hydrogen bonds between the complex and solvent molecules may be obtained. As before, Gd-bonded carboxylate/phosphonate and free O atoms can be distinguished. The distance limit is fixed at $r_{OH} = 2.2$ Å.

That hydrogen bond lifetimes (Table 6) are shorter than the mean residence times in the second coordination shell can be explained by the possible jumping of water molecules from one donor O atom to another without leaving the second coordination shell. Indeed, we observed a rather high frequency for water molecules (Table 7) simultaneously hydrogen-bonded to two carboxylate/phosphonate O atoms. For the free O atoms $O_f$ the ability to bond to more water molecules than the coordinating oxygen $O_c$ (hydration number $q_f > q_c$) is balanced by a greater lability (the hydrogen bond lifetime is shorter).

Table 6. Hydrogen bond number and lifetime around coordinating ($O_c$) and free ($O_f$) carboxylate/phosphonate oxygens.

| Complex | $q(O_c)$ | $\tau_M$ [ps] | $q(O_f)$ | $\tau_M$ [ps] |
|---|---|---|---|---|
| $[Gd(teta)]^-$ | 1.1 | 8.9 | 1.9 | 4.5 |
| $[Gd(dota)(H_2O)]^-$ | 1.0 | 14.7 | 2.3 | 6.8 |
| $[Gd(dotp)]^{5-}$ | 1.6 | 27.8 | 2.7 | 27.7 |
| $[Gd(dtpa)(H_2O)]^{2-}$ | 1.1 | 9.0 | 2.6 | 7.8 |
| $[Gd(dtpa\text{-}bma)(H_2O)]$ | 0.7 | 13.9 | 2.1 | 6.1 |

Table 7. Probability for water molecules to form two hydrogen bonds simultaneously.

| Complex | $O_c$ [%] | $O_f$ [%] |
|---|---|---|
| $[Gd(teta)]^-$ | 17.3 | 9.7 |
| $[Gd(dota)(H_2O)]^-$ | 34.5 | 10.3 |
| $[Gd(dotp)]^{5-}$ | 92.0 | 22.4 |
| $[Gd(dtpa)(H_2O)]^{2-}$ | 54.8 | 27.1 |
| $[Gd(dtpa\text{-}bma)(H_2O)]$ | 49.4 | 14.0 |

### Complexes with acyclic ligands

**Structural results**: Unlike their macrocyclic counterparts, the acyclic ligand complexes $[Gd(dtpa)(H_2O)]^{2-}$ and $[Gd(dtpa\text{-}bma)(H_2O)]$ do not have the benefit of high symmetry. Therefore we present only average values over the whole space for the radial distribution around the $Gd^{3+}$ ion (Figure 8). We observed the same general features as for the macrocyclic compounds: the position of the first peak of the H rdf is closer to the metal than that of the O rdf. However, the

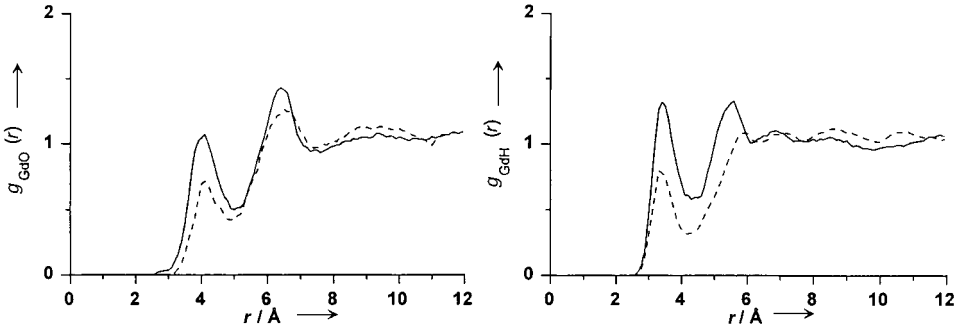


Figure 8. The rdf for water O atoms (left) and H atoms (right) around Gd of $[Gd(dtpa)(H_2O)]^{2-}$ (——) and $[Gd(dtpa\text{-}bma)(H_2O)]$ (- - - -).

average number of water molecules present in the second coordination shell (Table 4) is higher than for the $[Gd(teta)]^-$, $[Gd(dota)(H_2O)]^-$, and $[Gd(dotp)]^{5-}$ complexes, consistently with a more extended bonding site. Indeed, the hydrophilic part of the complex is proportionally larger for the acyclic complexes. The ligand occupies eight sites in the capped square antiprism geometry, five of which are used by carboxylate/amide O atoms in the acyclic ligands (compared with only four in the macrocyclic ligands). The second-shell coordination number is higher for the doubly charged $[Gd(dtpa)(H_2O)]^{2-}$ than for the neutral $[Gd(dtpa\text{-}bma)(H_2O)]$.

**Influence of the inner-sphere water molecule on the second coordination shell**: Since the dipole orientation of the water in the second coordination shell water is almost the opposite of that of the inner-sphere water molecule, one may wonder about the interaction of the latter with water molecules belonging to the second shell. The radial distribution of solvent water around the inner-sphere water protons (Figure 9) has a peak near 2.0 Å, with a following minimum at 2.3 Å. The height of the peak depends on the ligand: it is quite strong for the $[Gd(dtpa)(H_2O)]^{2-}$ complex, but almost disappears for $[Gd(dtpa\text{-}bma)(H_2O)]$ and only a shoulder is observable for $[Gd(dota)(H_2O)]^-$. We calculated the occurrence of hydrogen bonds between the inner-sphere water molecule and the solvent using a geometrical definition. Besides a distance criterion $r_{H_{is}-O_{solvent}} < 2.3$ Å given by the first minimum of the rdf of solvent oxygen around the inner-sphere water hydrogen, a further angular condition $\Theta_{O_{is}\text{-}H_{is}\text{-}O_{solvent}} < 30^\circ$

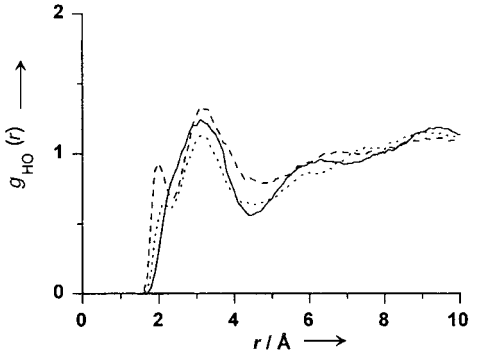


Figure 9. The rdf for water O atoms around inner-sphere water H atoms of $[Gd(dtpa)(H_2O)]^{2-}$ (----), $[Gd(dtpa\text{-}bma)(H_2O)]$ (····), and $[Gd(dota)(H_2O)]^{-}$ (——).

was required to define a hydrogen bond[34, 38] (Figure 10). The results show that inner-sphere water indeed interacts with the second-shell water molecules, since 10–30% of the stored configurations (depending on the ligand) show second-shell water molecules bonded to it in this way (Table 8).

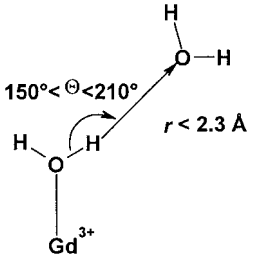


Figure 10. Criteria for hydrogen bonding between inner-sphere and outer-sphere water.

Table 8. Hydrogen bonding probability for the inner-sphere water molecule.

| Complex | [%] |
|---|---|
| $[Gd(dota)(H_2O)]^{-}$ | 13.8 |
| $[Gd(dtpa)(H_2O)]^{2-}$ | 30.3 |
| $[Gd(dtpa\text{-}bma)(H_2O)]$ | 21.4 |

**Dynamic results**: The dynamic hydration parameters of $[Gd(dtpa)(H_2O)]^{2-}$ and $[Gd(dtpa\text{-}bma)(H_2O)]$ were very similar to those of $[Gd(dota)(H_2O)]^{-}$ and $[Gd(teta)]^{-}$. Again, residence times were 20–25 ps with respect to the metal center ion (Table 5), and around 10 ps for the hydrogen bond lifetimes (Table 6).

The similarity of macrocyclic and acyclic ligand chelates in this respect allows the preliminary generalization that a second coordination shell involving a small number of water molecules in fast exchange (20–30 ps residence time) with the bulk water seems to be a feature of gadolinium (and probably other lanthanide) polyaminocarboxylates. Ligands of this type appear to differ only in the number of water molecules involved. However, the example of $[Gd(dotp)]^{5-}$ shows that modification of the functional groups of the ligand can produce significant changes in the residence time of water molecules in the second coordination shell.

**Calculation of the outer-sphere relaxivity from molecular dynamics simulations**

Outer-sphere relaxivity of $^1H$ spins is usually described using Freed's analytical force-free model,[3, 4] assuming a free relative diffusion of water molecules in the neighborhood of the paramagnetic center. In the light of the MD results presented so far this assumption is not valid for our systems. We have checked the consequences of this apparently invalid approximation, and compared the predictions of the simulations with the experimental data obtained so far.

Freed's general translational diffusion model incorporates the standard equation given by Abragam[39] for the dipole–dipole relaxation of a nuclear spin $I$ interacting with an electronic spin $S$ [Eq. (4)] and calculates spectral density functions $J(\omega)$ from the Smoluchowski diffusion equation [Eq. (5)].

$$\frac{1}{T_{1dd}} = \frac{4}{15}\pi S(S+1)\gamma_I^2\gamma_e^2\hbar^2\left(\frac{\mu_0}{4\pi}\right)^2 N_A \frac{[Gd^{3+}]}{1000}\{3J_0(\omega)+7J_1(\omega)\} \quad (4)$$

$$\frac{\partial P(r_0|r,t)}{\partial t} = D\nabla\cdot\left[\nabla P(r_0\,|\,r,t)+\frac{1}{kT}P(r_0\,|\,r,t)\nabla U(r)\right] \quad (5)$$

The spectral density functions $J(\omega)$ are calculated by means of Abragam's time–correlation function [Eq. (6)], where $\Pi$ is the average number density.

$$G(t) = \frac{4}{15}\Pi\int d^3r\int d^3r_0 D^{(2)}_{0m}(\Omega_r)D^{(2)}_{0m}(\Omega_{r0})P(r_0\,|\,r,t)g(r_0)/r_0^3 r^3$$
$$J(\omega) = 2\mathrm{Re}\int_0^\infty e^{i\omega t}G(t)dt \quad (6)$$

The potential of mean force $U(r)$ between two particles is related to the radial distribution function through Equation (7).

$$\ln g(r) = -\frac{U(r)}{kT} \quad (7)$$

Thus intermolecular forces can be taken into account for arbitrary radial distributions. However, an analytical form of $J(\omega)$ can only be obtained for the simplest models, such as free diffusion. This is the approximation made by Freed in the widely applied force-free model. In the general case it is possible to perform a numerical calculation based on finite difference methods. Instead of a continuous diffusion as described by the Smoluchowski equation, let us consider a succession of finite jumps between discrete distances $r_i$. One can then reformulate the problem of evaluating $J(\omega)$ as in Equations (8) and (9).[4]

$$[-\mathbf{W}+\mathbf{B}-1/T_{ie}\mathbf{1}-i\omega 1]Q = \bar{R} \quad (8)$$

$$J(\omega) = 2\Pi\sum_{i=0}^{N}\frac{\Delta r_i}{r_i^2}\mathrm{Re}(Q_i) \quad (9)$$

The matrix equation given by Hwang and Freed[4] does not include the electron relaxation rate $1/T_{ie}$, but comparison of the derivations of the analytical equations with and without this contribution leads straightforwardly to Equation (8). **W** is the transition probability matrix between discrete values of the distance $r$, whose elements include free diffusion and the force derived from the potential $U(r)$.[4] The elements of the



0947-6539/01/0703-0606 $ 17.50+.50/0 *Chem. Eur. J.* **2001**, *7*, No. 3

various matrices and vectors are given by Equations (10) and (11).

$$R_i = g(r_i)/r_i^2 \tag{10}$$

$$B_{ij} = \delta_{ij} 6D/r_i^2 \tag{11}$$

where $D$ is the diffusion coefficient ($22.36 \times 10^{-9}\ m^{-2}s^{-1}$ for water at room temperature[40]). Thus if the average diffusion coefficient and electron relaxation rate are known, calculation of the spectral distribution function $J(\omega)$ from the radial distribution function $g(r)$ is simply a matter of solving the matrix Equation (8) to find the elements of $Q(r)$. Continuous variation of $\omega$ then leads to the calculation of the nuclear magnetic relaxation rate $1/T_1$ as a function of the observation frequency: that is, the nuclear magnetic resonance dispersion (NMRD) profile.

Besides the structural information provided by the rdf, one also needs to know the electronic relaxation rate $1/T_{ie}$ as a function of the observation frequency $\omega$. In the last few years several equations have been proposed to account for the electronic relaxation of $Gd^{III}$ chelates,[41–45] with varying success. In the following calculations we used the approach and parameters of Powell et al.,[27] where simplified expressions provide an adequate description of the electron relaxation [Eqs. (12) and (13)] and spin rotation [Eq. (14)] contributions to the $^1H$ and $^{17}O$ nuclear magnetic relaxation of these complexes.

$$\frac{1}{T_{2e}} = \Delta^2 \tau_v \left( \frac{5.26}{1 + 0.372\omega_e^2 \tau_v^2} + \frac{7.18}{1 + 1.24\omega_e \tau_v} \right) \tag{12}$$

$$\frac{1}{T_{1e}} = \frac{1}{25} \Delta^2 \tau_v \{4S(S+1) - 3\} \left( \frac{1}{1 + \omega_e^2 \tau_v^2} + \frac{4}{1 + 4\omega_e^2 \tau_v^2} \right) \tag{13}$$

$$\frac{1}{T_{eSR}} = \frac{\delta g^2}{9\tau_R} \tag{14}$$

In spite of the clear weaknesses identified by Powell et al.,[27] they have the advantage of relative simplicity.

A custom-made program (available upon request) based on Equations (4)–(13) was developed for the calculation of the outer-sphere relaxivity from the rdf and electron relaxation equations. For $[Gd(dota)(H_2O)]^-$, $[Gd(dtpa)(H_2O)]^{2-}$, and $[Gd(dtpa\text{-}bma)(H_2O)]$ we have compared our calculations with the estimated outer-sphere contribution given by the simultaneous $^{17}O$ NMR/NMRD/EPR fitting procedure of Powell et al., who used Freed's force-free model (Table 9). Experimental room-temperature NMRD profiles are reported when no inner-sphere contribution exists ($[Gd(teta)]^-$ and $[Gd(dotp)]^{5-}$). The $[Gd(dotp)]^{5-}$ NMRD profile was taken from the literature,[46] whereas $[Gd(teta)]^-$ was measured in-house.

Table 9. Electronic relaxation and diffusion parameters used in the simulation of NMRD profiles.

| Complex | $\Delta^2$ [$10^{19}s^{-2}$] | $\tau_v$ [ps] | $\delta g^2$ | $\tau_R$ [ps] | $D_{GdH}$ [$10^{-10}m^{-2}s^{-1}$] | $a_{GdH}$ [Å] |
|---|---|---|---|---|---|---|
| $[Gd(teta)]^{-}$ [a] | 9 | 16 | 0 | – | – | – |
| $[Gd(dota)(H_2O)]^{-}$ [b] | 1.6 | 11 | 0.019 | 77 | 20.2 | 3.5 |
| $[Gd(dotp)]^{5-}$ [a] | 0.9 | 11 | 0.019 | 77 | – | – |
| $[Gd(dtpa)(H_2O)]^{2-}$ [b] | 4.6 | 25 | 0.012 | 58 | 20 | 3.5 |
| $[Gd(dtpa\text{-}bma)(H_2O)]$ [b] | 4.1 | 25 | 0.008 | 66 | 23 | 3.5 |

[a] Electronic parameters from fit to the experimental NMRD data. [b] Parameters from ref. [27].

The outer-sphere relaxivity profile calculated for $[Gd(dota)(H_2O)]^-$ and $[Gd(dtpa\text{-}bma)(H_2O)]$ using the general model compare favorably with Freed's force-free model, with the advantage that it is not necessary to guess the distance of closest approach $a_{GdH}$ (Figure 11). Freed's analytical force-free model can be used as an empirical relationship, involving two parameters, $D_{GdH}$ and $a_{GdH}$. In practice, the closest approach distance $a_{GdH}$ is fixed at a reasonable value and the relative diffusion constant $D_{GdH}$ is adjusted. The parameters extracted from this model are only effective ones, however, with no direct physical meaning.

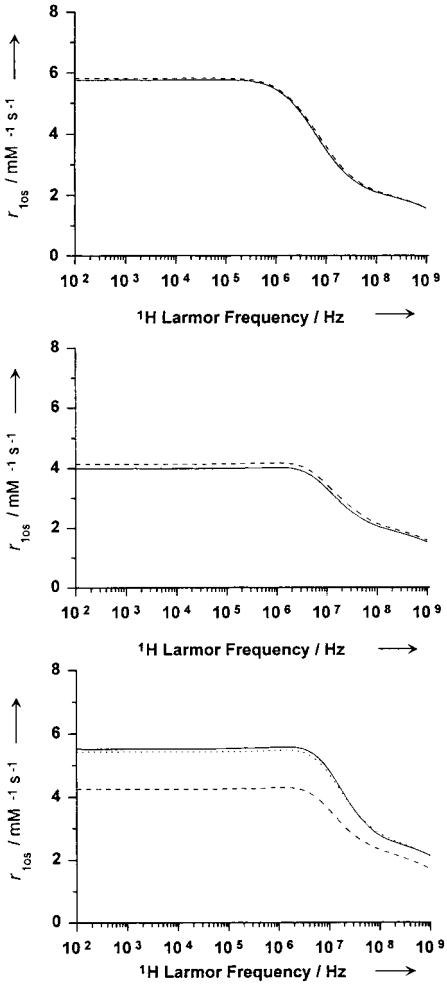


Figure 11. Outer-sphere relaxivity profile of $[Gd(dota)(H_2O)]^-$ (top), $[Gd(dtpa\text{-}bma)(H_2O)]$ (middle), and $[Gd(dtpa)(H_2O)]^{2-}$ (bottom) from MD simulations (——), from Freed's force-free model (- - - -), and with $a_{GdH} = 3.0$ Å (····).

In the case of $[Gd(dtpa)(H_2O)]^{2-}$, our calculated low-field relaxivity is 20% higher than the value obtained using Powell's empirical parameters. This discrepancy can be removed by reducing the closest approach distance in Powell's model from its typical value of 3.5 Å to 3.0 Å, which is significantly lower than the Gd–H distance for the first

maximum of the rdf (3.4 Å) and should be considered as an effective parameter only. $[Gd(dtpa)(H_2O)]^{2-}$ is the only compound in our study for which the rdf peak of the second shell rises well above unity (Figure 1right and Figure 8right), corresponding to 12.8 protons in the second shell (Table 4). The higher calculated relaxivity might be explained by the presence of a significant number of protons at $r < 3$ Å compared with $[Gd(dota)(H_2O)]^-$ and [Gd(dtpa-bma)-$(H_2O)$]. The residence time of water molecules in the second shell of $[Gd(dtpa)(H_2O)]^{2-}$ is in the same range as for the other polyaminocarboxylates, so the only apparent difference is the number of these molecules. It is possible that our simulations overestimate the second-shell hydration number in this case. However, since no direct experimental data are available, it is impossible at this stage to compare the respective accuracy of the experimental and theoretical estimates.

Since direct experimental measurements are possible for $[Gd(teta)]^-$ and $[Gd(dotp)]^{5-}$, they clearly require a more detailed discussion. The NMRD profile obtained for $[Gd(teta)]^-$ with the $[Gd(dota)(H_2O)]^-$ electronic parameters is essentially the same as for $[Gd(dota)(H_2O)]^-$, about twice as high as the experimental profile (Figure 12). It was only

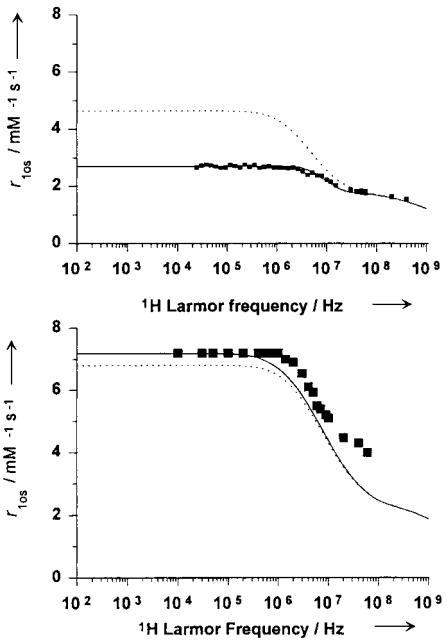


Figure 12. NMRD profile of $[Gd(teta)]^-$ (top) and $[Gd(dotp)]^{5-}$ (bottom); ····, profiles incorporating the electron relaxation parameters determined by Powell et al. for $[Gd(dota)(H_2O)]^-$.

possible to reproduce the rather low $[Gd(teta)]^-$ relaxivity ($2.8\,mM^{-1}s^{-1}$ at 0.02 MHz) by drastically changing the electronic parameters from those of $[Gd(dota)(H_2O)]^-$. As a crude visual fitting procedure, we set the trace of the square of the zero-field splitting operator $\Delta^2$ to $9 \times 10^{19}$ $s^{-2}$. This leads to a much faster electron spin relaxation than that obtained by Powell et al. for $[Gd(dota)(H_2O)]^-$, thus significantly reducing the relaxivity. Preliminary X-band (9.425 G Hz) EPR measurements indicated that the electron spin relaxation of $[Gd(teta)]^-$ was indeed extremely fast, with a linewidth ten times as high as $[Gd(dota)(H_2O)]^-$ (Figure 13). In this respect $[Gd(teta)]^-$ is definitely not such a good model of the outer-sphere relaxivity of $[Gd(dota)(H_2O)]^-$ as it is sometimes said to be.[2] A more complete analysis of the properties of this compound is beyond the scope of this work.

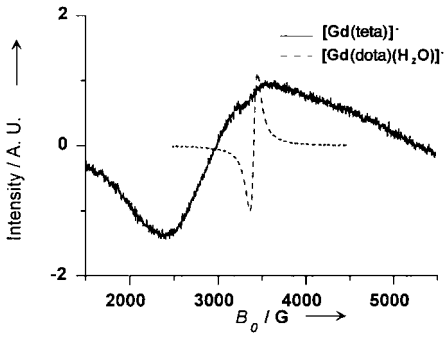


Figure 13. Room-temperature X-band EPR spectra of $[Gd(teta)]^-$ and $[Gd(dota)(H_2O)]^-$.

The NMRD profile we have calculated for $[Gd(dotp)]^{5-}$ with the $[Gd(dota)(H_2O)]^-$ parameters is only 6% too low ($6.8$ instead of $7.2\,mM^{-1}s^{-1}$ at 0.01 MHz). Aime et al.[46] obtained a good fit of their NMRD data using two contributions: Freed's force-free model with $a_{GdH} = 3.76$ Å ($r_{1os} = 3.3\,mM^{-1}s^{-1}$at 0.1 MHz), and an inner-sphere-like contribution with hydration number $q = 1$ and a residence time of 3000 ps. Our results indicate that such a long correlation time is not necessary, as we are already able to account for the major part of the observed relaxivity in terms of our second-shell data (with a much shorter residence time of 56 ps). The low-field part of the profile is correctly reproduced after a slight adjustment of the electron spin parameters (results of the fitting procedure are reported in Table 9), but the agreement is not exact at higher fields. Admittedly our structural model of $[Gd(dotp)]^{5-}$ is not perfect. The calculated Gd–N distance (3.0 Å; Table 2) is significantly longer than the observed distances in similar polyaminocarboxylate and polyaminophosphinate complexes (typically 2.6–2.7 Å). Furthermore the possible presence of counterions in close contact with the complex, as shown, for example, by Sherry using $^{23}Na$ NMR spectroscopy,[47] would certainly affect the second coordination shell. Taking counterions into account in the simulation would greatly increase the computational cost, however, requiring a much larger periodic box. Even more fundamentally, the discrepancy at higher field may well originate in the inadequacy of the model of relaxation through translational diffusion for this complex. Indeed, the residence time we have observed in the second shell of $[Gd(dotp)]^{5-}$ (56 ps) is not negligible with respect to the usual rotational correlation time of such complexes (60–80 ps[27]). Thus a purely translational diffusive motion (as described by Smoluchowski's equation) might not be strictly valid in this case.

In the case of the macrocyclic complexes, the partial rdf for the hydrophilic and hydrophobic regions (Figure 3) enables us to estimate their respective contributions to the outer-sphere relaxivity. Depending on the complex, the hydrophilic con-



0947-6539/01/0703-0608 $ 17.50+.50/0 *Chem. Eur. J.* **2001**, *7*, No. 3

tribution increases from 63% of the overall low-field outer-sphere relaxivity for $[Gd(teta)]^-$ to 71% for $[Gd(dota)(H_2O)]^-$ and 73% for $[Gd(dotp)]^{5-}$.

## Conclusion

We have investigated the outer-sphere hydration of polyaminocarboxylate and polyaminophosphonate gadolinium chelates, for which a force-free model had previously been assumed in the analysis of magnetic resonance experiments. A more realistic description is necessary for a better understanding of the nuclear relaxation properties of aqueous solutions of these compounds.

Beyond the structural differences of the complexes studied, there are similarities that extend to other compounds of the same class. A few water molecules are hydrogen-bonded to the hydrophilic groups of the ligand (their exact number depends on the number of such residues available for bonding), forming a second coordination shell. The behavior of this second shell is therefore highly dependent on the charge distribution of the $Gd^{III}$ chelate. Depending on the ligand, the structure can be highly anisotropic, as for the complexes of the macrocyclic ligands $teta^{4-}$, $dota^{4-}$, and $dotp^{8-}$. These water molecules have a very short lifetime in this second shell compared with that in the inner sphere, typically 20–25 ps for polyaminocarboxylate complexes in contrast to microseconds for an inner-sphere water molecule. The water molecules surrounding the hydrophobic part of the complexes are randomly oriented and their lifetime approaches that of water for self-diffusion in neat water (3 ps[10]). As can be seen from the example of $[Gd(dotp)]^{5-}$ the use of different ligand types (such as polyaminophosphonates) can increase the outer-sphere relaxivity by stabilizing the second coordination shell. Furthermore, due to the anisotropy of this hydration shell, the hydrophilic side of the complex can be the source of as much as 73% of the outer-sphere relaxivity at low field.

We have demonstrated the limitations of Freed's force-free model for some complexes, notably $[Gd(dotp)]^{5-}$. We can relate our results to experimental data through a numerical approach based on Freed's general model, including electron spin relaxation. By a method based on finite differences, one can calculate spectral density functions from the readily available radial distribution function $g(r)$. Our results are in general agreement with the experimental data without the need to introduce too many adjustable parameters. However, a quantitative agreement in all cases will only be possible when the electron spin relaxation is further elucidated.

## Acknowledgements

We thank Dr. T. Kowall (University of Lausanne) and Dr. O. Schafer (Institute of Inorganic Chemistry, University of Fribourg) for their help initially. We appreciate the financial support of the Swiss National Science Foundation and the Office for Education and Science (OFES). This research was carried out in the framework of the EC D18 Action "Lanthanide Chemistry for Diagnosis and Therapy".

[1] R. B. Lauffer, *Chem. Rev.* **1987**, *87*, 901–927.
[2] P. Caravan, J. J. Ellison, T. J. McMurry, R. B. Lauffer, *Chem. Rev.* **1999**, *99*, 2293–2352.
[3] J. H. Freed, *J. Chem. Phys.* **1978**, *68*, 4034–4037.
[4] L.-P. Hwang, J. H. Freed, *J. Chem. Phys.* **1975**, *63*, 4017–4025.
[5] J. W. Chen, R. L. Belford, R. B. Clarkson, *J. Phys. Chem. A* **1998**, *102*, 2117–2130.
[6] M. Botta, *Eur. J. Inorg. Chem.* **2000**, 399–407.
[7] T. Kowall, F. Foglia, L. Helm, A. E. Merbach, *J. Am. Chem. Soc.* **1995**, *117*, 3790–3799.
[8] T. Kowall, F. Foglia, L. Helm, A. E. Merbach, *J. Phys. Chem.* **1995**, *99*, 13078–13087.
[9] T. Kowall, F. Foglia, L. Helm, A. E. Merbach, *Chem. Eur. J.* **1996**, *2*, 285–294.
[10] A. Bleuzen, F. Foglia, E. Furet, L. Helm, A. E. Merbach, J. Weber, *J. Am. Chem. Soc.* **1996**, *118*, 12777–12787.
[11] R. Fossheim, S. G. Dahl, *Acta Chem. Scand.* **1990**, *44*, 698–706.
[12] R. Fossheim, H. Dugstad, S. G. Dahl, *J. Med. Chem.* **1991**, *34*, 819–826.
[13] D. E. Reichert, R. D. Hancock, M. J. Welch, *Inorg. Chem.* **1996**, *35*, 7013–7020.
[14] U. Cosentino, G. Moro, D. Pitea, A. Villa, P. C. Fantucci, A. Maiocchi, F. Uggeri, *J. Phys. Chem. A* **1998**, *102*, 4606–4614.
[15] E. S. Henriques, M. Bastos, C. F. G. C. Geraldes, M. J. Ramos, *Int. J. Quantum Chem.* **1999**, *73*, 237–248.
[16] O. Schafer, C. Daul, *Int. J. Quantum Chem.* **1997**, *61*, 541–546.
[17] B. H. Besler, K. M. J. Merz, P. A. Kollman, *J. Comput. Chem.* **1990**, *11*, 431–439.
[18] M. J. Frisch, G. W. Trucks, H. B. Schlegel, P. M. W. Gill, B. G. Johnson, M. A. Robb, J. R. Cheeseman, T. A. Keith, G. A. Petersson, J. A. Montgomery, K. Raghavachari, M. A. Al-Laham, V. G. Zakrewski, J. V. Ortiz, J. B. Foresman, J. Cioslowski, B. B. Stefanov, A. Nanayakkara, M. Challacombe, C. Y. Peng, P. Y. Ayala, W. Chen, M. W. Wong, J. L. Andres, E. S. Replogle, R. Gomperts, R. L. Martin, D. J. Fox, J. S. Binkley, D. J. Defrees, J. Baker, J. J. P. Stewart, M. Head-Gordon, C. Gonzalez, J. A. Pople, Gaussian 94, Gaussian, Inc., Pittsburgh (PA), **1995**.
[19] M.-R. Spirlet, J. Rebizant, M.-F. Loncin, J. F. Desreux, *Inorg. Chem.* **1984**, *23*, 4278–4283.
[20] C. A. Chang, L. C. Francesconi, M. F. Malley, K. Kumar, J. Z. Gougoutas, M. F. Tweedle, *Inorg. Chem.* **1993**, *32*, 3501–3508.
[21] T.-Z. Jin, S.-F. Zhao, G.-X. Xu, Y.-Z. Han, N.-C. Shi, Z.-S. Ma, H. Xuebao, *Acta Chim. Sinica* **1991**, *49*, 569.
[22] G. Jamieson, , Nycomed–Salutar, Inc. **1990**.
[23] M. Dolg, H. Stoll, A. Savin, H. Preuss, *Theor. Chim. Acta* **1989**, *75*, 173–194.
[24] E. J. Baerends, Amsterdam Density Functional (ADF), Scientific Computing and Modelling, Amsterdam, **1997**.
[25] A. D. Becke, *J. Chem. Phys.* **1986**, *85*, 7184–7187.
[26] J. Perdew, *Phys. Rev. B* **1986**, *33*, 8822–8824.
[27] D. H. Powell, O. M. Ni Dubhghaill, D. Pubanz, L. Helm, Y. S. Lebedev, W. Schlaepfer, A. E. Merbach, *J. Am. Chem. Soc.* **1996**, *118*, 9333–9346.
[28] S. Aime, M. Botta, M. Fasano, M. P. M. Marques, C. F. G. C. Geraldes, D. Pubanz, A. E. Merbach, *Inorg. Chem.* **1997**, *36*, 2059–2068.
[29] W. L. Jorgensen, J. Chandrasekhar, J. D. Madura, R. W. Impey, M. L. Klein, *J. Chem. Phys.* **1983**, *79*, 926–935.
[30] W. F. van Gunsteren, H. J. C. Berendsen, GROMOS86, Biomolecular Software, Groningen, **1986**.
[31] J.-P. Ryckaert, G. Ciccoti, H. J. C. Berendsen, *J. Comput. Phys.* **1977**, *23*, 327–341.
[32] H. J. C. Berendsen, J. P. M. Postma, W. F. van Gunsteren, A. DiNola, J. R. Haak, *J. Chem. Phys.* **1984**, *81*, 3684–3690.
[33] R. W. Impey, P. A. Madden, I. R. McDonald, *J. Phys. Chem.* **1983**, *87*, 5071–5083.
[34] A. Luzar, D. Chandler, *J. Chem. Phys.* **1993**, *98*, 8160–8173.
[35] S. G. Kalko, E. Guàrdia, J. A. Padró, *J. Phys. Chem. B* **1999**, *103*, 3935–3941.
[36] M. Sunnerhagen, V. P. Denisov, K. Venu, A. M. J. J. Bonvin, J. Carey, B. Halle, G. Otting, *J. Mol. Biol.* **1998**, *282*, 847–858.
[37] A. M. J. J. Bonvin, M. Sunnerhagen, G. Otting, W. F. van Gunsteren, *J. Mol. Biol.* **1998**, *282*, 859–873.

[38] M. Ferrario, M. Haughney, I. R. McDonald, M. L. Klein, *J. Chem. Phys.* **1990**, *93*, 5156 – 5166.
[39] A. Abragam, *The Principles of Nuclear Magnetism*, Clarendon Press, Oxford, **1961**.
[40] R. Mills, *J. Phys. Chem.* **1973**, *77*, 685 – 688.
[41] D. H. Powell, A. E. Merbach, G. Gonzalez, E. Brücher, K. Micskei, M. F. Ottaviani, K. Köhler, A. von Zelewsky, O. Y. Grinberg, Y. S. Lebedev, *Helv. Chim. Acta* **1993**, *76*, 2129 – 2146.
[42] T. I. Smirnova, A. I. Smirnov, R. L. Belford, R. B. Clarkson, *J. Am. Chem. Soc.* **1998**, *120*, 5060 – 5072.
[43] E. Strandberg, P.-O. Westlund, *J. Magn. Reson. A* **1996**, *122*, 179 – 191.
[44] S. Rast, P. H. Fries, E. Belorizky, *J. Chim. Phys.* **1999**, *96*, 1543 – 1550.
[45] A. Borel, É. Tóth, L. Helm, A. Jánossy, A. E. Merbach, *Phys. Chem. Chem. Phys.* **2000**, *2*, 1311 – 1318.
[46] S. Aime, M. Botta, E. Terreno, P. L. Anelli, F. Uggeri, *Magn. Reson. Med.* **1993**, *30*, 583 – 591.
[47] A. D. Sherry, *J. Alloys Compd.* **1997**, *249*, 153 – 157.

Received: July 6, 2000 [F2587]



0947-6539/01/0703-0610 $ 17.50+.50/0